# Role of conductivity in the electrohydrodynamic patterning of air-liquid interfaces

P. Gambhire and R. M. Thaokar
*Department of Chemical Engineering, Indian Institute of Technology Bombay**
(Received 2 March 2012; revised manuscript received 30 May 2012; published 4 September 2012)

The effect of electrical conductivity on the wavelength of an electrohydrodynamic instability of a leaky dielectric-perfect dielectric (LD-PD) fluid interface is investigated. For instabilities induced by dc fields, two models, namely the PD-PD model, which is independent of the conductivity, and the LD-PD model, which shows very weak dependence on the conductivity of the LD fluid, have been previously suggested. In the past, experiments have been compared with either of these two models. In the present work, experiments, analytical theory, and simulations are used to elucidate the dependence of the wavelength obtained under dc fields on the ratio of the instability time ($\tau_s = 1/s_{\max}$) and the charge relaxation time ($\tau_c = \epsilon\epsilon_0/\sigma$, where $\epsilon_0$ is the permittivity of vacuum, $\epsilon$ is the dielectric constant, and $\sigma$ is the electrical conductivity). Sensitive dependence of the wavelength on the nondimensional conductivity $S_2 = \sigma_2\mu_2 h_0^2/(\epsilon_0^2\phi_0^2\delta^2)$ (where $\sigma_2$ is the electrical conductivity, $\mu_2$ is the viscosity, $h_0$ is the thickness of the thin liquid film, $\phi_0$ is the rms value of the applied field, and $\delta$ is a small parameter) is observed and the PD-PD and the LD-PD cases are observed only as limiting behaviors at very low and very high values of $S_2$, respectively. Under an alternating field, the frequency of the applied voltage can be altered to realize several regimes of relative magnitudes of the three time scales inherent to the system, namely $\tau_c$, $\tau_s$, and the time period of the applied field, $\tau_f$. The wavelength in the various regimes that result from a systematic variation of these three time scales is studied. It is observed that the linear Floquet theory is invalid in most of these regimes and nonlinear analysis is used to complement it. Systematic dependence of the wavelength of the instability on the frequency of the applied field is presented and it is demonstrated that nonlinear simulations are necessary to explain the experimental results.

DOI: 10.1103/PhysRevE.86.036301 PACS number(s): 47.20.Ma, 47.65.−d, 47.54.−r

## I. INTRODUCTION

With the advent of miniaturization, it has become more and more important to be able to produce devices with micron- to submicron-sized structures at a mass scale inexpensively. In this regard, researchers have been working on a new technique which uses the instabilities formed at a fluid-fluid interface under electric fields to form micron-sized patterns and grooves in polymeric films. The activity in this area began with the pioneering experiments of Schaffer *et al*. [1], who studied the instability at an air-polystyrene interface under a dc field. They observed that a thin polymer film destabilized to form columns, which grew to touch the top plate (electrode) and on subsequent rapid quenching, froze into solid structures. The columns formed in a perfect hexagonal arrangement with a constant center-to-center spacing ($\lambda$). They also proposed a simple model wherein a balance of the forces due to surface tension (stabilizing) and those due to the electrostatic pressure (destabilizing) led to an expression for the wavelength of the instability. Subsequent experimental studies focused on reducing the column spacing further by making use of a second liquid as the top fluid instead of air [2,3], using a patterned mask to obtain features of desired shapes [4], using air-polymer-polymer trilayers to obtain hollow or core-shell kinds of structures [5–7], and using low-viscosity polymers to reduce the time scales of the formation [8].

The experimental studies were almost simultaneously complemented by the development of the theoretical model. Early research groups studied the instability in the linear regime under the lubrication approximation considering the fluids to be either perfect dielectrics (PD), i.e., materials with absolutely no free charge [9], or leaky dielectrics (LD), materials with an infinitesimal amount of charge [10,11]. The inclusion of a small amount of charge in the fluid was found to increase the wave number and the growth rate of the instability considerably. These studies were followed by nonlinear simulations in 2D by Craster and Matar [12] for an LD system and in 3D by Verma *et al*. [13] and Wu and Russel [14] for a PD system. The latter studied the effect of different mask shapes (triangular, square, and so on) and showed that the patterns differed in each case.

From the above-reviewed literature the authors make note of a few points. The linear theory for a PD-PD and an LD-PD system has been extensively studied now for over a decade but a systematic experimental validation has not yet been reported. Experimentalists have been working with polymer systems which have low albeit finite conductivity (leaky dielectric materials) and yet they have been comparing the results to the PD-PD theory [1–3,8,15,16]. Under a dc field, even the low charge present in a fluid accumulates at the interface and the system has to be described by a leaky dielectric model. A PD material can be realized in experiments only by an alternating field at high frequencies, that is, when the time period of the alternating field ($\tau_f = 1/\omega$, where $\omega$ is the frequency of the alternating field) is significantly small compared to the time for charge migration ($\tau_c = \epsilon_0\epsilon/\sigma$, where $\epsilon_0$ is the permittivity of vacuum, $\epsilon$ is the dielectric constant of fluid film, and $\sigma$ is the conductivity).

For that matter, it is difficult to judge *a priori* if the system under study is a PD-PD system or an LD-PD system. If the charge relaxation time ($\tau_c$) is at least an order of magnitude larger than the time taken for the growth of the instability ($\tau_s$), a PD system can be realized even with a dc field. Hence, a

*rochish@che.iitb.ac.in

 

TABLE I. A summary of the time scales in a typical air-polymer system.

| Group | Schaffer *et al.* [15] | Schaffer *et al.* [15] | Lin *et al.* [2] |
|---|---|---|---|
| Polymer | Polystyrene | Polystyrene | Polyisoprene |
| Conductivity (S/m) | $1 \times 10^{-12}$ | $1 \times 10^{-12}$ | $2.57 \times 10^{-15}$[a] |
| Viscosity (Pa-s) | 50[a] | 50[a] | 40 |
| Surface tension (N/m$^2$) | 0.03 | 0.03 | 0.032 |
| App. potential (V) | 30 | 50 | 20 |
| Film thickness (m) | $93 \times 10^{-9}$ | $120 \times 10^{-9}$ | $140 \times 10^{-9}$ |
| Electrode spacing (m) | $450 \times 10^{-9}$ | $1280 \times 10^{-9}$ | $1.08 \times 10^{-6}$ |
| $\tau_c$ (s) | 22.13 | 22.13 | 8161.28 |
| $\tau_{s_{\mathrm{LD}}}$ (s) | 9.3 | 5.71 | 7672.95 |
| $\tau_{s_{\mathrm{PD}}}$ (s) | 48.81 | 29.96 | 23926.98 |

[a]Values taken from the polymer data handbook [17].

knowledge of the conductivity of the fluids, which has been neglected hitherto, is quite essential. To exemplify the point further, in Table I, a compilation of the charge migration times of different polymers widely used in the literature is given. Also the growth rates predicted by the LD theory and the PD theory for the same system have been calculated. Although, it can be observed from this data that the charge would have accumulated at the interface during the time for the instability growth predicted by a PD theory rendering the system an LD system, experiments in these references have been compared to the PD theory. From the above discussion, it is evident that a knowledge of the competition among the different time scales (namely $\tau_c$, $\tau_s$, and $\tau_f$) is quite essential for an accurate prediction of the instability.

A detailed study of the dependence of the wavelength of instability as a function of the conductivity of the liquid film is missing in the literature, a possible reason being that the linear theory predicts a weak dependence on conductivity. But, as noted by Shankar and Sharma [11], the linear LD theory might predict inaccurate values of wavelength at low values of conductivities. At high charge migration times (i.e., low values of conductivity) the charge accumulation at the interface will not have reached a steady state, in contrast to the assumption made in the linear leaky dielectric theory, which is the reason for the inaccuracy. Also, while $\tau_s$ scales as $\mu_2 h_0^2/(\epsilon_0 \phi_0^2 \delta^2)$ (where $\mu_2$ is the viscosity and $h_0$ is the thickness of the liquid film, $\epsilon_0$ is the relative permittivity of vacuum, $\phi_0$ is the rms value of the applied field, and $\delta$ is a small parameter), $\tau_c$ is independent of voltage. Thus, even for a particular fluid for a given electrode configuration, the ratio of time scales can change considerably by just changing the voltage. Therefore, a theory which goes beyond the linear PD-PD and linear LD-PD is required.

Nonlinear analysis can be used as an alternative to the linear theory. In the past, nonlinear analysis was carried out only to get structural information of the instability and to simulate the effect of patterned electrode configurations. As the evolution of an infinitesimal random initial perturbation is studied by direct numerical integration without linearizing the system, the assumptions made in the linear theory are overcome using the nonlinear analysis.

Experiments in the past have been exploratory rather than a validation of the theory. Systematic experiments to ascertain the relative effect of the three time scales on the instability have not been carried out so far. Moreover, although the instability under dc fields has been extensively addressed in the literature it was only recently that Roberts and Kumar [18] studied the instability under alternating fields by carrying out both linear and nonlinear analysis for an air-liquid interface. Experimental validation of the effect of frequency on the wavelength of the instability has not been reported yet. Also Roberts and Kumar [18] studied only a particular regime of the time scales, i.e., $\tau_c \ll \tau_f < \tau_s$. Experiments, though, can possibly be beyond this regime.

In the present work, the following issues are addressed: (1) What will the actual wavelength observed under dc fields be and will it depend on conductivity, unlike the prediction of linear theory, which shows a poor dependence on the conductivity? (2) Can this behavior be validated using experiments? (3) Do experiments support the theory given by Roberts and Kumar [18]? (4) Are there experimental regimes which have not been explained by Roberts and Kumar [18]? and (5) Can one explain such experimental results? An exhaustive study of all the regimes of time scales, namely the charge relaxation time ($\tau_c$), the time taken for the growth of the instability ($\tau_s$), and the time period of the applied alternating field ($\tau_f$), which affect the final dimensions of the instability, is carried out by making use of the linear PD and LD theories, Floquet theory, nonlinear analysis, and experiments for the same.

In the next section, the system under study and the leaky dielectric model equations under the lubrication approximation are described. The details of the nonlinear analysis and experiments are provided next and a comparison among the linear theory, nonlinear analysis, and experiments is made.

## II. MODEL

### A. System description

The system consists of a layer of air on top of a viscous Newtonian liquid film held between planar electrodes (refer Fig. 1). The longitudinal direction is denoted by $x^*$ while a voltage of rms value $\phi_0$ is applied along the transverse direction, i.e., the $y^*$ direction. The variations in the third direction ($z$) are not considered and a 1D analysis is conducted. The upper fluid is referred to as 1 and the lower fluid as 2. The viscosity, density, conductivity, and dielectric constant of the upper fluid are denoted by $\mu_1$, $\rho_1$, $\sigma_1$, and $\epsilon_1$, respectively,

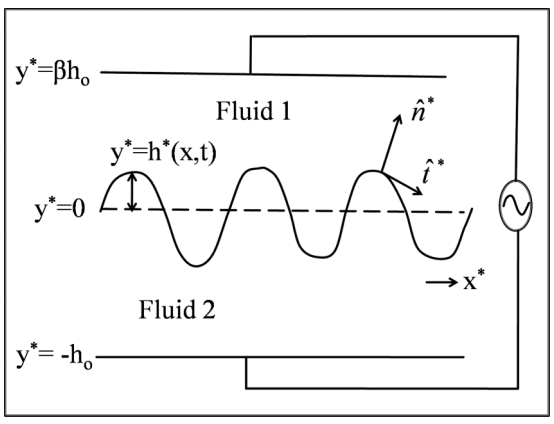


FIG. 1. A schematic of the fluid-fluid interface under electric field.

and those of the lower fluid by $\mu_2$, $\rho_2$, $\sigma_2$, and $\epsilon_2$. The position of the interface is denoted by $y^* = 0$ while the electrodes are held at $y^* = \beta h_0$ and $y^* = -h_0$, where $h_0$ is the thickness of the lower film. $\hat{n}$ and $\hat{t}$ denote the unit normal and tangential vectors, respectively, and the superscript $*$ denotes dimensional quantities which are values of properties bearing a physical dimension or unit. Once they have been scaled or divided by an appropriate parameter they are termed non-dimensional or dimensionless.

### B. Thin-film approximation

The leaky dielectric theory with the thin-film approximation (TFA) is used to model the system under study. In the present work the following parameters are used to scale the variables in the system. Length in the $y$ direction is scaled by the film thickness $h_0$. A balance of the destabilizing electrical stress given by $\epsilon_0\phi_0^2/h_0^2$ and the stabilizing stress due to surface tension, given by $\gamma h_0/L^2$, gives the natural length scale for the instability, $L = (\frac{\gamma h_0^3}{\epsilon_0\phi_0^2})^{1/2}$. A small parameter $\delta = \frac{h_0}{L} = (\frac{\epsilon_0\phi_0^2}{\gamma h_0})^{1/2}$ is obtained as a ratio of the two length scales $h_0$ and $L$. The thin-film approximation assumes that this parameter is very small. Therefore, asymptotically expanding all the equations in $\delta$ and retaining only the $O(1)$ terms simplifies the analysis to a great extent. Tangential velocity ($u$) is scaled by $\epsilon_0\phi_0^2\delta/(\mu_2 h_0)$ and from the continuity equation the scaling for the normal velocity ($v$) is obtained as $\epsilon_0\phi_0^2\delta^2/(\mu_2 h_0)$. Substituting these scalings in the $x$ direction Stokes equation, the scaling for pressure is obtained to be $\epsilon_0\phi_0^2/h_0^2$. The scaling for time under dc fields is $\mu_2 h_0^2/(\epsilon_0\phi_0^2\delta^2)$ and that under ac fields is $1/\omega$. Interfacial charge is scaled by $\epsilon_0\phi_0/h_0$ and conductivity is scaled by $\epsilon_0^2\phi_0^2\delta^2/(\mu_2 h_0^2)$.

The governing equations and the boundary conditions of the leaky dielectric model using the thin-film approximation have been described in a previous publication by the authors [19] and are also given in the appendix for reference. The governing equations [Eqs. (A16)–(A18)] and the boundary conditions [Eqs. (A19)–(A27)] are solved such that all the system variables like $u,v,\phi$ are in terms of the position of the interface $h(x,t)$. The procedure followed is as described by Shankar and Sharma [11] for dc fields and Roberts and Kumar [18] and Gambhire and Thaokar [19] for ac fields to obtain evolution equations for the interfacial position $h(x,t)$ and interfacial charge $q(x,t)$.

## III. NONLINEAR ANALYSIS

The evolution equations of the interface position [Eq. (A26)] and the charge conservation [Eq. (A27)] obtained after carrying out the procedure outlined in Sec. II B are numerically integrated to obtain $h$ as a function of $x$ and $t$. The nonlinear analysis is carried out in MATLAB. A grid of length $x = 40\pi$ is used and is divided into 200 points. The value of the initial condition is defined at each of these 200 points. The spatial derivatives are determined using the finite difference approach and periodic boundary conditions are used at the edges. The initial condition is a small random number perturbation and the integration in time is carried out using an in-built ordinary differential equation solver ode15s. The output interfacial position ($h$) is plotted as a function of $x$ and $t$. A sample plot from the simulations is shown in Fig. 2. The plot shows $h(x,t)$ as a function of $x$. The wavelength is calculated from this plot as the mean of the peak-to-peak spacing between each of columns. In all the nonlinear simulation results presented in this work, the initial free charge at the interface is assumed to be zero.

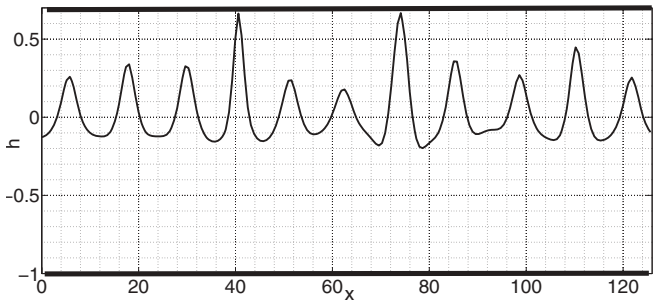


FIG. 2. Sample results from the nonlinear analysis under dc fields. The dark lines at the top and the bottom of the graph denote the electrodes. The parameters used are $\epsilon_1 = 1, \epsilon_2 = 3, \beta = 0.7, S_1 = 0$, and $S_2 = 0.003$. The nondimensional time at which this snapshot is obtained is $t = 202$. The peak-to-peak spacing gives the scaled wavelength.

## IV. EXPERIMENTAL

### A. Materials

Indium tin oxide (ITO) coated microscopic glass slides ($25 \times 75 \times 1.1$ mm) were purchased from Delta Technologies (Loveland, CO, USA). Silicone oil bearing the brand name Dow Corning Corporation 200 fluid of viscosity 30,000 cSt (verified with measurements using MCR 301, Anton Paar GmbH) at 25 °C was procured from Sigma Aldrich (Mumbai, India).

### B. Methods

The ITO-coated glass slides were used as electrodes. Two pieces of scotch tape [thickness ∼42 $\mu$m measured using a surface profilometer (Dektak Veeco)] were stuck along the breadth of one of the slides (slide 1) with a 4-cm separation between them. The tape acted as the spacer between the electrodes. Around 0.2 ml of silicone oil was spread on the slide 1 and then spun at 3000 rpm for 130 s on a spin coater (Photoresist Spinner PRS-6K, Ducom Instruments, Bangalore, India). The thickness of the formed film was estimated from the difference in the weights of the slide before and after coating the film and knowing the area of slide coated. The mean thickness obtained after following this protocol was $\approx 36.1 \pm 0.8$ $\mu$m. The second slide was then placed on top of the first slide separated by the spacers. A second layer of scotch tape, stuck breadthwise on the first layer of the tape only on one side of the slide 1, gave a wedge shaped gap between the two electrodes. Air trapped in the space between the silicone oil layer and the top electrode formed the top fluid. The device was connected to a function generator (Model 33220A, Agilent Technologies, CA, USA) through a high-voltage amplifier (Model 5/80, 1000 V/V gain, Trek, Inc., New York, USA). A digital SLR camera (Model D90, Nikon) was used to image the formed columns. The center-to-center spacing

between the columns was measured using the NIS-elements BR Image analysis software from Nikon. The conductivity and permittivity of the silicone oil sample were measured using impedance spectroscopy (using a liquid sample cell, BDS 1308, Novocontrols, Germany). The permittivity was found to be $\approx 2.65 \pm 0.007$ while the conductivity was found to vary with frequency (refer to Fig. 11). These changing values of conductivity were taken into account while comparing the experimental results with the theory. In experiments, it is difficult to change the conductivity of the leaky dielectric fluid while keeping all the other properties constant. Hence, the nondimensional conductivity $[S_2 = \sigma_2\mu_2 h_0^2/(\epsilon_0\phi_0\delta)^2]$ was experimentally varied by changing the voltage applied to the system. On increasing the voltage, lower values of conductivity (nondimensional) can be achieved. The zero conductivity (PD limit) was achieved by carrying the same experiments at a higher frequency of 1 kHz. This was much higher than the typical inverse charge relaxation time of the system ($\sigma/\epsilon\epsilon_0 \sim 0.1$ Hz).

## V. RESULTS AND DISCUSSION

### A. dc fields

When a system is subjected to a dc field, there are two physically relevant time scales in the system, namely the time taken by the instability to grow ($\tau_s = 1/s_{\max}$, where $s_{\max}$ is the maximum growth rate of the instability) and the charge relaxation time ($\tau_c = \epsilon_0\epsilon/\sigma$). An interplay between these time scales shows a variety of behavior in the system. The nondimensional conductivity $S_2 = \frac{\sigma/\epsilon_0}{(\epsilon_0\phi_0^2\delta^2)/(\mu_2 h_0^2)} = O(\frac{\tau_s}{\tau_c})$. Thus, the relative magnitude of the instability time and the charge relaxation time can be altered by changing the nondimensional conductivity of the lower fluid. All the possible cases are discussed next.

#### 1. $\tau_c \gg \tau_s$ regime

This denotes a case where charges migrate negligibly from their position during the time it takes for the instability to form. Hence, no free charge accumulates at the interface and the instability can be described by the perfect dielectric theory. This regime is realized when $S_2 \ll 1$ as seen in Fig. 3.

#### 2. $\tau_c \ll \tau_s$ regime

Under this condition, the charge accumulation at the interface of the fluids is instantaneous. During the time the instability grows, the system experiences a constant value of charge accumulated at the interface, which is responsible for tangential Maxwell's stresses. The instability in such a case can be best described using a leaky dielectric theory. This regime is realized when $S_2 \gg 1$, as seen in Fig. 3.

The above two cases have been exhaustively discussed in the literature.

#### 3. $\tau_c \simeq \tau_s$ regime

Linear stability analysis of a PD-PD system assumes that the base state is devoid of free charge while an LD-PD analysis assumes there is enough charge at the interface in the base state such that the field in the lower fluid is zero. In other words, the bottom fluid is like a perfect conductor in the base

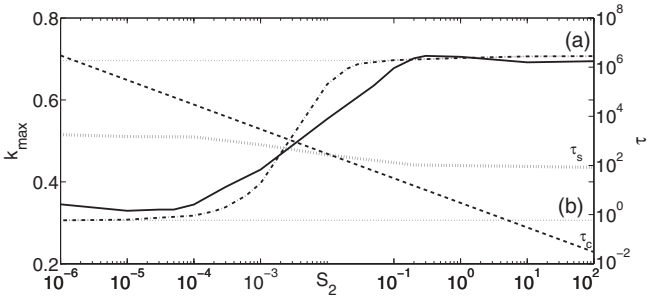


FIG. 3. The variation of $k_{\max}$ and $\tau$ with change in conductivity of the lower fluid $S_2$ for $\beta = 1$. The $(\cdots)$ lines (a) and (b) represent the results from the LD-PD and PD-PD linear theories, respectively, the $(- \cdot -)$ line curve denotes results from the LD modified theory, and the solid line denotes the results from the nonlinear analysis. The $(- - -)$ line ($\tau_c$) represents the values of the charge relaxation time, $\tau_c$, while the $(\cdots)$ line ($\tau_s$) represents the time for the growth of the instability, $\tau_s$, for the present case. The values of parameters are $\epsilon_1 = 1$, $\epsilon_2 = 3$, $\mu_r = 10^{-7}$, $S_1 = 0$, and $\beta = 1$.

state. Typical experimental systems though have a low but finite value of conductivity. Typical polymers used for pattern formation in the past have been very low conductivity polymers (see Table I). The charge relaxation times of such polymers ($\tau_c$) are quite high. The other time scale in the system, the time required for the growth of the instability ($\tau_s$), is of the same order as that of the charge relaxation time in such systems. The result being that the system does not behave like a leaky dielectric because the interfacial charge has not reached its steady-state value in the base state nor does it behave like a perfect dielectric material due to the infinitesimal charge accumulation existent in the system. This case was discussed by Shankar and Sharma [11] previously. They mentioned that the linear theory cannot be used in cases where the top fluid is air (i.e., $\epsilon_1 = 1$ and $S_1 = 0$) or a similar perfect dielectric while the lower fluid is a very low conductivity material. They give an expression for the base state charge evolution at an interface as $q(t) = [1 - \exp(-\frac{S_2\beta t}{1+\beta\epsilon_2})]/\beta$. To describe the limit when the charge buildup time is finite [neither too small (LD-PD) nor too long (PD-PD)], a simple model is proposed in the present work referred to as the *LD modified theory*. In this model, it is assumed that the time taken by charge accumulation in the "base state" is the time that a PD instability would take to set in. Therefore, the time in the expression for $q(t)$ is taken as the inverse growth rate for a PD-PD system. The expression for base charge reduces to $q = [-1 + \exp(-\frac{12(1+\beta\epsilon_2)^5 S_2}{(1-\epsilon_2)^4\epsilon_2^2})]/\beta$. The linear stability analysis is now conducted with this base charge and compared to the linear LD dc theory.

The nonlinear analysis in which the charge evolution equation naturally takes into account the buildup of charge at the interface is also used to study this limit. For the model system of air (fluid 1) and silicone oil (fluid 2) which is also relevant to several other air-dielectric systems, since the dielectric constant values vary between 2 and 5 for most of the fluids used in experiments [17], the values of the parameters (after scaling) are taken to be $\epsilon_1 = 1$, $\epsilon_2 = 3$, $\mu_r = 10^{-7}$, and $S_1 = 0$. To study this limit, the conductivity of the lower fluid ($S_2$) is varied over 6 orders of magnitude and

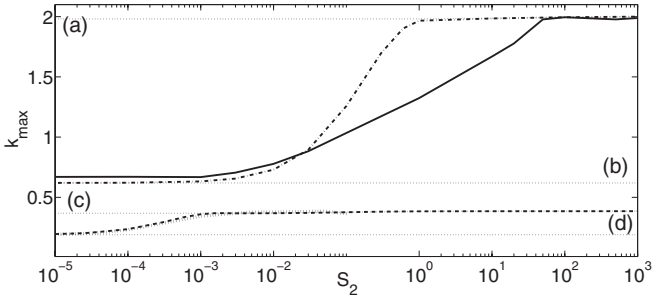


FIG. 4. The variation of $k_{\max}$ with $S_2$ for $\beta = 0.5$ and 1.5. The values of parameters are $\epsilon_1 = 1$, $\epsilon_2 = 3$, $\mu_r = 10^{-7}$, and $S_1 = 0$. The $(\cdots)$ lines (a) and (c) represent the results from the LD-PD theory for $\beta = 0.5$ and $\beta = 1.5$, respectively. The $(\cdots)$ lines (b) and (d) represent the results from the PD-PD theory for $\beta = 0.5$ and $\beta = 1.5$, respectively. The solid curve and the $(\cdots)$ curve represent the results from the nonlinear analysis and the $(- \cdot -)$ curve and the $(- - -)$ curve represent the results from the LD modified theory for $\beta = 0.5$ and $\beta = 1.5$, respectively.

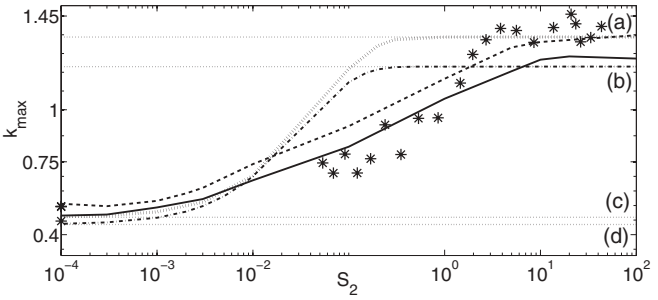


FIG. 5. A comparison of $k_{\max}$ as a function of $S_2$ between results obtained from experiments and nonlinear analysis. The values of the parameters used in the theoretical analysis are $\epsilon_1 = 1$, $\epsilon_2 = 3$, $\mu_r = 10^{-7}$, and $S_1 = 0$. The $(\cdots)$ lines (a) and (b) indicate the linear LD-PD theory and the $(\cdots)$ lines (c) and (d) indicate the PD-PD theory for $\beta = 0.65$ and $\beta = 0.7$, respectively. The $(\cdots)$ line curve and the $(- \cdot -\cdot)$ line curve represent the results from the LD modified theory for $\beta = 0.65$ and $\beta = 0.7$, respectively, while the $(- - -)$ curve and the solid line curve represent the results from the nonlinear analysis for $\beta = 0.65$ and $\beta = 0.7$, respectively. The $*$ symbols indicate experimental results.

the fastest-growing wave number, $k_{\max}$, is determined for every value. The results are plotted in Fig. 3 for the case when $\beta = 1$. The dotted line (a) in Fig. 3 represents the results from the linear LD-PD theory while the dotted line (b) in Fig. 3 indicates the PD-PD theory. The $k_{\max}$ for a perfect dielectric material is independent of the conductivity of the fluid. The linear LD-PD theory shows a decrease in $k_{\max}$ with decreasing $S_2$ although, the reduction, over several decades of conductivities, is quite low. This is because the base state for an LD-PD system, as assumed in the linear theory, is really a conductor on account of the infinite time available for charge buildup at the interface. Therefore, the base state electric field in the bottom fluid is zero and independent of the conductivity in the LD-PD linear theory. In contrast, the results from the nonlinear analysis show a drastic decrease in $k_{\max}$ with decreasing values of conductivity. At very low values of conductivity (limiting to zero), the charge migration time (indicated by dashed line ($\tau_c$) in Fig. 3) is high, i.e., $\tau_c \gg \tau_s$ (indicated by dotted line ($\tau_s$) in Fig. 3), and a limiting PD behavior is seen. As the conductivity increases, the two time scales become almost of the same order. At such competing time scales, the system begins experiencing accumulation of charge at the interface, which gives rise to tangential Maxwell's stresses and, hence, the instability can no longer be explained by the simple PD theory. At high-enough conductivities, $\tau_c \ll \tau_s$, the system behaves as a leaky dielectric fluid. It should be noted that the time available for charge buildup in the LD modified theory is assumed to be of $O(1)$, which is the time scale of the instability.

Figure 4 shows the variation of $k_{\max}$ with $S_2$ as a function of $\beta$, the ratio of the thicknesses of the two fluids. As is already known [11], $k_{\max}$ decreases with increasing $\beta$. This is because the field experienced at the film surface becomes weaker as the air gap becomes larger. It is also seen that the match between the $k_{\max}$ values predicted by the linear and the nonlinear analysis extends to lower values of conductivity with increasing air gap. The reason for this could be attributed to the fact that as $\beta$ increases, the time required for the growth of the instability increases, allowing sufficient time for the charges to migrate to the interface, resulting in a leaky dielectric behavior.

Although the PD-PD and the LD-PD linear theories fail to predict the $k_{\max}$ when $\tau_c \approx \tau_s$ the LD modified theory seems to work reasonably well, especially at higher values of $\beta$. At lower $\beta$ though, there is an appreciable difference between the predictions of the nonlinear analysis and the LD modified theory. Thus, to compare experimental data, nonlinear analysis is the best tool available.

The above theoretical analysis predicts that even in dc experiments, the wavelength observed should critically depend on the nondimensional conductivity $S_2$. Therefore, experimental results cannot be naively compared with the PD-PD or the LD-PD theories as has been done in the literature [1–3,8,15,16]. To validate the claim that conductivity indeed has an effect on the wavelength of the formed instability, a set of experiments were carried out under dc field. As mentioned earlier, a change in the conductivity (nondimensional) was achieved by changing the voltage applied to the system. Changing voltage actually aids in changing the value of $\tau_s$ with respect to $\tau_c$ which, in turn, helps in experimental realization of the regimes of the time scales discussed above. Figure 8 shows the variation of the wavelength of the instability from experiments as a function of the applied voltage. As the applied voltage is increased, the columns became denser, indicating a smaller wavelength. The pattern and order were observed to improve with increasing voltage.

In the past, experiments have almost always been compared with a linear perfect dielectric theory. A leaky dielectric theory predicted only a weak dependence on conductivity. From the discussion in this section, it is evident that the instability depends critically on the value of the nondimensional conductivity of the lower fluid. The results from the experiments were, therefore, scaled and compared to the LD modified theory and the nonlinear analysis, carried out for the same parameters used in the experiments in Fig. 5. Experimentally, the value of $\beta$ varied between 0.65 and 0.7 and, hence, the results from the linear theories and the nonlinear analysis are reported at these boundary values. No other fitting parameter was used. The

results from the nonlinear analysis are shown by the solid line ($\beta = 0.7$) and dashed line ($\beta = 0.65$) while the experimental results are denoted by asterisks. The effect of competing time scales is clearly evident through experiments. At low values of $S_2$, the PD-PD theory [dotted line (c) for $\beta = 0.65$ and the dotted line (d) for $\beta = 0.7$] seems to predict the experimental data well while at high values of $S_2$ the LD-PD theory [dotted lines (a) for $\beta = 0.65$ and (b) for $\beta = 0.7$] is more appropriate. At intermediate values of $S_2$ [$O(1)$], the LD modified theory [the dotted curve (for $\beta = 0.65$) and the dash-dot curve (for $\beta = 0.7$)] suggested in this work, qualitatively explains the data. Better quantitative agreement, though, is observed by comparison with the results from the nonlinear analysis. The experimental data for $S_2 < 0.05$ could not be obtained as it corresponded to the highest voltage (160 V) that could be used without damaging the conductive ITO coating of the glass slides.

### B. ac field

When a system is subjected to an alternating field, apart from $\tau_c$ and $\tau_s$, an additional time scale becomes significant, namely the time period of the applied alternating field ($\tau_f = 1/\omega$). For a perfect dielectric material, the alternating polarity of the electrodes does not alter the nature or the dynamics of the instability (which is equivalent to a dc instability under an rms value of the field [18,20]). But for a leaky dielectric material, the charge migration depends on the polarity of the electrode and, hence, the instability depends on how rapidly it alternates. An extensive study of all the different parametric regimes possible among these three time scales is discussed next.

In the Fig. 6 the variation of $k_{\max}$ as a function of the nondimensional frequency $\Omega$ is presented at different conductivities ($S_2$) using both nonlinear analysis and linear Floquet theory. Nonlinear analysis is carried out for the case

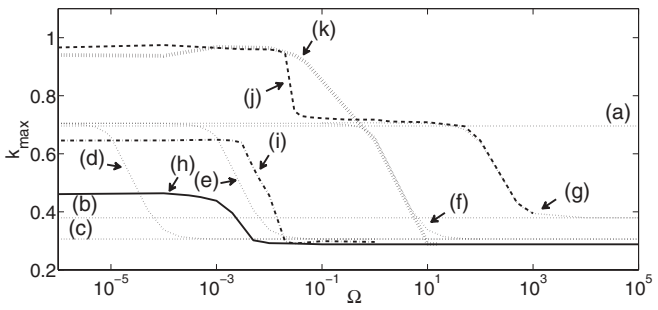


FIG. 6. $k_{\max}$ plotted as a function of $\Omega$ to study the effect of the interplay of the three time scales ($\tau_f$, $\tau_c$, and $\tau_s$) on the formed instability. The values of the parameters are $\epsilon_1 = 1$, $\epsilon_2 = 3$, $\mu_r = 10^{-7}$, $\beta = 1$, and $S_1 = 0$. The $(\cdots)$ lines (a) and (c) denote the results from the linear LD-PD (for $S_2 = 10$) and the PD-PD theory under dc fields, respectively. The $(\cdots)$ line curves (d), (e), and (f) denote the results from Floquet theory while the solid line curve (h), the $(- \cdot -)$ line curve (i), and the $(\cdots)$ curve (k) denote results from the nonlinear analysis for $S_2 = 10^{-4}$, $10^{-2}$, and 10, respectively. The $(\cdots)$ curve (g) and the $(- - -)$ curve (j) represents results from Floquet theory and nonlinear analysis obtained using parameters from Roberts and Kumar [18], i.e., $\epsilon_1 = 1$, $\epsilon_2 = 4$, $\mu_r = 0$, $\beta = 1$, $S_1 = 0$, and $S_2 = 10^3$.

of an applied ac field using the procedure outlined in Sec. III. The applied potential is taken to be of the form $\phi_p \cos(\omega t)$, where $\phi_p = \sqrt{2}\phi_0$. In the linear regime, the effect of ac fields is studied using the Floquet analysis. The Floquet analysis assumes a well-developed time-periodic base state with a time-periodic free charge distribution. The general characteristic of a system subjected to an ac field is that the instability carries the signature of a leaky dielectric material at low frequencies and a perfect dielectric material at high frequencies, the transition occurring at a frequency corresponding approximately to the inverse charge relaxation time ($f_{\text{trans}} = 1/\tau_c$). The results from the Floquet theory in the present study have already been benchmarked against the results of Roberts and Kumar [18] by the authors in a previous publication [19].

#### 1. $\tau_c \ll \tau_s$

This case corresponds to the regime where the charge relaxation is instantaneous compared to the time for instability. For $\tau_c \ll \tau_s$, one can further have $\tau_f < \tau_s$, i.e., the field alternates faster than the time taken by the instability to grow, or $\tau_f > \tau_s$, i.e., the instability grows before the applied field completes a cycle.

$\tau_f < \tau_c \ll \tau_s$. This case indicates a regime where the instability takes the longest to form. The field alternates significantly during that time but the charge takes a longer time to migrate to the interface. As the field alternates before the charge migrates there is no net charge accumulation at the interface and the system behaves like a perfect dielectric material. This case is the high-frequency limiting case for all the conductivities presented in Fig. 6 and agrees with the PD-PD dc theory represented by the dotted lines (b) and (c) in Fig. 6.

$\tau_c < \tau_f \ll \tau_s$. This case also indicates a regime where the instability takes the longest to form. The field alternates significantly during that time but the charge migration occurs even before the field completes a cycle. The system now behaves likes a leaky dielectric material under an ac field [low-frequency region of the curve (g) in Fig. 6].

The above two cases are similar to those studied previously by Roberts and Kumar [18]. They form the limiting cases for a leaky dielectric material under an ac field. As the frequency of the applied field is increased (or the time period reduced), the system goes from a leaky dielectric behavior to a perfect dielectric behavior. The limiting cases are easily obtained from the linear stability analysis of a perfect dielectric material [curves (b) and (c) in Fig. 6] and a leaky dielectric material [curve (a) in Fig. 6] subjected to a dc field of an rms voltage $\phi_0$, respectively. The variation of $k_{\max}$ and $s_{\max}$ with frequency $\Omega$ has been obtained using Floquet theory with an applied field of $\phi_p = \sqrt{2}\phi_0$. The behavior of a very high conductivity fluid ($S_2 = 10^3$) (as considered by Roberts and Kumar [18], curve (g) in Fig. 6) indeed shows these limits.

$\tau_c \ll \tau_s < \tau_f$. This case indicates a regime where the time period of the applied field is higher than the time taken by the instability to form. This is a common case seen experimentally at very low frequencies. As the undulations grow, the instability is realized even before the field alternates a single cycle. The interface thus experiences a varying field in the course of $\tau_s$. As one goes to lower frequencies, the system experiences an almost constant voltage whose magnitude is

dependent on the type of waveform applied. For example, for the current case of a cosine waveform, the voltage is equivalent to the peak voltage of the cycle (i.e., $\sqrt{2}\phi_0$). Floquet theory, described in Sec. A4b, is based on the assumption that the system experiences a steady alternating field with a rms amplitude ($\phi_0$) ($\tau_f \ll \tau_s$) and, hence, fails in determining the wavelength of the instability in this regime. This regime is indicated by the curve (k) in Fig. 6. The values of parameters used are $\epsilon_1 = 1$, $\epsilon_2 = 3$, $\mu_r = 10^{-7}$, $\beta = 1$, $S_1 = 0$, and $S_2 = 10$. At high frequencies, when the system behaves as a PD, a good agreement is seen between the linear and nonlinear theories. Similarly, at intermediate frequencies, too, a good agreement is seen between Floquet theory and the nonlinear theory. In contrast, at low frequencies, the value of $k_{\max}$ is seen to increase above the value predicted by the linear LD theory, and plateau to a new higher value of $k_{\max}$. This value could be predicted using a linear LD theory in which the peak value of the applied field is used as a scaling parameter. As one goes to lower frequencies, the instability occurs even before the completion of a single cosine cycle. Hence, within the time scale of the instability the system experiences a higher field than the rms value. The wavelength of the instability is inversely proportional to the applied field and varies as $\lambda \propto E_0^{-3/2}$. This leads to a higher value of $k_{\max}$ than that predicted by the linear theory. In fact, even for the case of the parameters used by Roberts and Kumar [18] [curve (g) in Fig. 6], a similar behavior is observed [curve (j) in Fig. 6] at low frequencies. In the discussion of the results under ac fields by Roberts and Kumar [18] (Fig. 6 therein), the very low frequency range is not explored and, therefore, the increase in the wave number was not observed.

#### 2. $\tau_c \gg \tau_s$

This case refers to the condition when the charge takes an infinitely long time to migrate to the interface when compared to the time the instability takes to form. Therefore, for either case of $\tau_f > \tau_s$ or $\tau_f < \tau_s$, the system always exhibits a perfect dielectric behavior. At high frequencies ($\tau_f < \tau_s$), the predictions agree with the dc PD-PD theory [curve (c) in Fig. 6]. At lower frequencies ($\tau_f > \tau_s$), a deviation from the PD-PD Floquet theory is observed. As discussed earlier, Floquet theory assumes a rms value of the applied alternating field even at very low frequencies when the system experiences an almost constant field (equivalent to the $\phi_p$). This limitation is overcome using the nonlinear analysis at these frequencies. The curve (h) in Fig. 6 is plotted using parameters $\epsilon_1 = 1$, $\epsilon_2 = 3$, $\mu_r = 10^{-7}$, $\beta = 1, S_1 = 0$, and $S_2 = 10^{-4}$. The larger wave number at lower frequencies is only due to a higher local voltage when $\tau s < \tau f$ [curve (h) in Fig. 6 in the low-frequency limit]. The system behaves like a PD-PD system for the frequency range shown in the figure. The transition from the low to high value of frequency regime occurs at $\tau_f \sim \tau_s$. Floquet theory, though, predicts this transition to occur at $\tau_f \sim \tau_c$.

#### 3. $\tau_c \sim \tau_s \sim \tau$

This case is analogous to the case discussed earlier under Section V A3 under the dc field regime. In this case, both the charge migration and growth of the instability occurred simultaneously. Under ac fields, two further cases occur when the third time scale $\tau_f$ is considered. The different cases are discussed next.

$\tau_f < \tau$. This denotes a case where the system experiences a field which alternates quickly. This is analogous to the PD behavior discussed earlier. As the field alternates its polarity even before the charges can respond to it, there is no net migration to the interface, rendering the system a perfect dielectric.

$\tau_f > \tau$. Under these conditions, the undulations grow while charges migrate to the interface during a single cycle of the applied field and experience the peak voltage in contrast to the rms value assumed by the linear Floquet theory. This violates both the time-periodic field and the steady-state value of base charge assumed by Floquet theory. Nonlinear analysis is, therefore, employed in this regime to determine $k_{\max}$ as a function of frequency $\Omega$. A low value of conductivity, $S_2 = 10^{-2}$, is chosen to study this limit. The $k_{\max}$ for this value of conductivity under a dc field obtained from the nonlinear analysis is lower than the value predicted by the linear LD-PD theory (Fig. 3). Therefore, under an ac field, at low frequencies, the value of $k_{\max}$ should plateau to a value lower than the one predicted by the linear theory. This aspect is captured by the nonlinear analysis. Curve (i) in Fig. 6 indicates this limit. A deviation in the results from the nonlinear analysis and those from the linear Floquet theory is seen at very low frequencies and, in this case, the value of $k_{\max}$ predicted by the nonlinear analysis is lower than that predicted by the linear LD-PD dc theory.

#### 4. *Comparison of experiments with theory*

The deviation of the nonlinear analysis from the linear theories in several of the above discussed regimes was validated by carrying out experiments within those regimes. The experiments were carried out as outlined in Sec. IV by varying the frequency and the results are plotted in Fig. 9 in the Appendix. In Fig. 7, experimental results have been

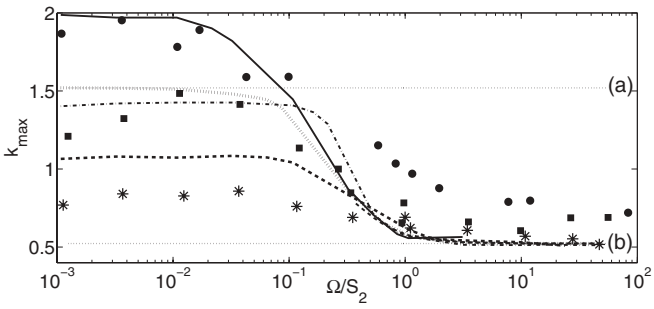


FIG. 7. A comparison of $k_{\max}$ as a function of $\Omega/S_2$ between results obtained from experiments and nonlinear analysis. The values of parameters used are $\epsilon_1 = 0$, $\epsilon_2 = 3$, $\mu_r = 10^{-7}$, $\beta = 0.6$, and $S_1 = 0$. The $(\cdots)$ lines (a) and (b) indicate results from the linear LD-PD and PD-PD theories, respectively, under dc fields. The $(\cdots)$ curve indicates collapse of results from Floquet theory for the three conductivity ranges 0.073–0.16, 1.17–2.56, and 18.73–41.08. The solid line curve, the $(- \cdot -)$ line curve, and the $(- - -)$ curve indicate results from the nonlinear analysis for the conductivity ranges 18.73–41.08, 1.17–2.56, and 0.073–0.16, respectively, while the corresponding experimental results are indicated by the symbols •, ■, and ∗.

plotted along with the results from the nonlinear analysis for three different ranges of conductivities (note: conductivity changes with frequency at a particular voltage). To sample three different values of conductivity, experimentally, in the same silicone oil fluid is difficult. An easier way, as discussed earlier, is to change the nondimensional conductivity (and, hence, the time scales) by changing the voltage applied to the system. Using the measured values of conductivity at each frequency (refer to Fig. 11), the nondimensional conductivity could be varied due to its sensitive dependence on the voltage ($S \sim \phi_0^{-2}$). In the present case we apply rms values of 35 V, 70 V, and 140 V to the system. $\phi_0 = 140$ V corresponds to the conductivity range $S_2 = 0.073$–$0.16$ (henceforth, the conductivity range mentioned corresponds to frequency ranging from $10^{-4}$ to 10 Hz), $\phi_0 = 70$ V corresponds to the conductivity range $S_2 = 1.17$–$2.56$, and $\phi_0 = 35$ V corresponds to the conductivity range $S_2 = 18.73$–$41.08$. These three ranges of conductivities were chosen such that the experimental time scales of the system could encompass several of the earlier discussed cases.

Figure 7 shows the variation of $k_{\max}$ with the nondimensional conductivity ($S_2$) and frequency ($\Omega$). The data at different nondimensional conductivities is seen to collapse when plotted as a function of $\Omega/S_2$. The results from Floquet theory are indicated by the dotted curve while the results from the LD-PD theory and PD-PD theory under dc fields are indicated by the dotted lines (a) and (b) in Fig. 7, respectively. Note that the LD-PD dc linear theory indicated by the line (a) in Fig. 7 is calculated for $S_2 = 18.73$–$41.08$. Due to the weak dependence of the LD-PD theory on $S_2$, the curves for the remaining two conductivity ranges fall on the same curve [curve (a) in Fig. 7] and, hence, are not reported here. The solid line indicates results from the nonlinear analysis for the value of $S_2 \sim 18.73$–$41.08$. It is qualitatively similar to the curve (k) in Fig. 6. Note that the simulations are carried out for the exact value of conductivity, which itself changes from a value of 18.73–41.08 from the low- to high-frequency limit. The • symbols indicate results from experiments for the same values of conductivity mentioned above. As discussed earlier, a deviation between the linear and nonlinear analysis is seen at low frequencies but a good agreement is seen between experiments and the nonlinear analysis, indicating that the wave number obtained, in experiments, in this regime is indeed higher than that predicted by the linear theory.

The results from the nonlinear analysis for the values of $S_2 \sim 1.17$–$2.56$ and $S_2 \sim 0.073$–$0.16$ are indicated by the dash-dot line curve and the dashed line curve, respectively. The $k_{\max}$ values for both these conductivities, at low frequencies, are seen to deviate from the linear LD dc values. These curves belong to the regimes indicated by the curve (i) and (h) in Fig. 6. The experimental results, indicated by the symbols ■ and $*$, respectively, are seen to agree well with the results from the nonlinear analysis.

The images from the experiments are shown in Fig. 10. The mismatch in the nonlinear analysis and the experimental results at high frequencies for the $\phi_0 = 35$ V case is attributed to the sparse columns formed at this voltage. It takes around 2–3 h for a row of columns to form and during this time it was observed that the columns formed previously, reposition slightly, affecting the overall ordering and resulting in a greater deviation in the measured mean wavelength. The order within the patterns was found to become better (hexagonal) as the voltage was increased.

## VI. CONCLUSIONS

In the present work, an extensive study of how an interplay among the three different time scales, namely the charge relaxation time ($\tau_c$), the time taken for the growth of the instability ($\tau_s$), and the time period of the applied field ($\tau_f$), affects the dimensions of the final structure of the instability. It was shown that the conductivity affects the wavelength of the formed instability and this dependence can be predicted by existing nonlinear analysis. A modified linear model also seems to predict the instability reasonably, although the conventional linear LD-PD and the linear PD-PD theories fail. The linear stability analysis, due to the assumption of instantaneous charge accumulation at the interface, can only be used to predict the limiting cases (as was done in the literature) of the parametric regime explored using the nonlinear analysis. This is demonstrated using dc experiments in which the nondimensional conductivity ($S_2$) is varied by changing the potential. Under ac fields, the waveform and the time period of the applied field were shown to have an effect on the formed instability. These effects were predicted using nonlinear analysis. The experiments and the simulations are found to be in reasonable agreement. It is shown that for these cases where the assumptions made in the linear theory are not satisfied, one has to resort to the nonlinear analysis. A naive comparison with the existing analytical theories thus could be erroneous.

## ACKNOWLEDGMENT

The authors acknowledge the financial assistance provided by the Department of Science and Technology, India.

## APPENDIX A: MODEL

The detailed governing equations and the boundary conditions used in the leaky dielectric model under the thin-film approximation are described here followed by the details of the linear stability analysis used for the case of the system under dc fields and the Floquet theory used for ac fields.

### 1. Governing equations

The equations governing the system are the continuity equation and the momentum balance equation for fluid flow and the Laplace equation for the electric potential,

$$\nabla^* \cdot \boldsymbol{V}_i^* = 0, \tag{A1}$$

$$\rho(\partial_t^* \boldsymbol{V}_i^* + \boldsymbol{V}_i^* \cdot \nabla^* \boldsymbol{V}_i^*) = -\nabla^* p_i^* + \mu_i \nabla^{*2} \boldsymbol{V}_i^*, \tag{A2}$$

$$\nabla^{*2} \phi_i^* = 0, \tag{A3}$$

where $p_i$ is the pressure, $\boldsymbol{V_i} = u\hat{\boldsymbol{e}}_x + v\hat{\boldsymbol{e}}_y$ is the velocity vector, $\rho$ and $\mu$ are the density and viscosity of the fluids, respectively, $\phi_i$ denotes the electric potential, and the subscript $i = 1,2$ refers to fluid 1 and fluid 2, respectively.

### 2. Boundary conditions

The following set of boundary conditions are used to solve the above equations: at the interface, velocities are continuous in the normal and tangential directions, i.e.,

$$(\boldsymbol{V_1}^* \cdot \hat{\boldsymbol{n}}) = (\boldsymbol{V_2}^* \cdot \hat{\boldsymbol{n}}), \tag{A4}$$

$$(\boldsymbol{V_1}^* \cdot \hat{\boldsymbol{t}}) = (\boldsymbol{V_2}^* \cdot \hat{\boldsymbol{t}}), \tag{A5}$$

where $\hat{\boldsymbol{n}}$ and $\hat{\boldsymbol{t}}$ are the unit normal and the unit tangential vectors, respectively, as indicated in Fig. 1, given by $\hat{\boldsymbol{n}} = \frac{-\partial_x h^* \hat{\boldsymbol{e}}_x + \hat{\boldsymbol{e}}_y}{\sqrt{1+\partial_x h^{*2}}}$ and $\hat{\boldsymbol{t}} = \frac{\hat{\boldsymbol{e}}_x + \partial_x h^* \hat{\boldsymbol{e}}_y}{\sqrt{1+\partial_x h^{*2}}}$. The operator $\partial$ with the subscripts $x$, $y$, or $t$ denotes differentiation with respect to that variable. $h(x,t)$ denotes the position of the interface and $\boldsymbol{V_1}$ and $\boldsymbol{V_2}$ are the velocity vectors for the two fluids. For an unperturbed interface, $\hat{\boldsymbol{n}} = \hat{\boldsymbol{e}}_{\boldsymbol{y}}$ and $\hat{\boldsymbol{t}} = \hat{\boldsymbol{e}}_{\boldsymbol{x}}$.

The stresses are balanced in the normal and tangential directions. In the normal direction the stresses satisfy

$$[\![\hat{\boldsymbol{n}} \cdot \boldsymbol{\tau}_{\boldsymbol{i}}^* \cdot \hat{\boldsymbol{n}}]\!] = \gamma \kappa^*, \tag{A6}$$

where the operator $[\![X]\!]$ denotes the jump $X_1 - X_2$ across the interface $h(x,t)$. $\gamma$ is the interfacial tension and $\kappa^* = \boldsymbol{\nabla} \cdot \hat{\boldsymbol{n}}$ is the curvature given by $\kappa^* = -\partial_x^2 h^*/(1+\partial_x h^{*2})^{3/2}$. The term on the right-hand side in Eq. (A6) represents the stabilizing force due to surface tension. The balance of stresses in the tangential direction is given by

$$[\![\hat{\boldsymbol{t}} \cdot \boldsymbol{\tau_i}^* \cdot \hat{\boldsymbol{n}}]\!] = 0, \tag{A7}$$

where $\boldsymbol{\tau}^*$, the total stress, i.e., the sum of the hydrodynamic and the electrical stresses, for the fluid $i$, is given by

$$\boldsymbol{\tau_i}^* = -p_i{}^* I + \mu_i(\boldsymbol{\nabla}^* \boldsymbol{V_i}^* + \boldsymbol{\nabla}^* \boldsymbol{V_i}^{*T}) + \boldsymbol{M_i}^*. \tag{A8}$$

The superscript $T$ indicates transpose, $i = 1,2$ denotes the two fluid layers, and $\boldsymbol{M_i}$ is the Maxwell stress tensor [21].

$$\boldsymbol{M_i}^* = \epsilon_i \epsilon_0 \left[\boldsymbol{E}_i^* \boldsymbol{E}_i^* - \tfrac{1}{2}(\boldsymbol{E}_i^* \cdot \boldsymbol{E}_i^*) I\right]. \tag{A9}$$

A balance of the tangential component of the electric field gives the continuity of the potentials across the interface

$$\phi_1^* = \phi_2^* \tag{A10}$$

and the balance of the normal component of electric field gives the electric displacement discontinuity

$$[\![\epsilon_0 \epsilon_i (-\boldsymbol{\nabla}^* \phi_i^* \cdot \hat{\boldsymbol{n}})]\!] = q^*, \tag{A11}$$

where $q$ is the interfacial charge. The dynamics of the position of the interface and the interfacial charge is given by the kinematic condition and the charge conservation equation, respectively,

$$\partial_t h^* + \boldsymbol{V_1}^* \cdot \boldsymbol{\nabla}^*{}_s h^* = v_2^* = v_1^*, \tag{A12}$$

$$\partial_t q^* + \boldsymbol{V_1}^* \cdot \boldsymbol{\nabla}^*{}_s q^* - q^* \hat{\boldsymbol{n}} \cdot (\hat{\boldsymbol{n}} \cdot \nabla^*) \boldsymbol{V_1}^* = [\![S_i^* \nabla^* \phi_i^* \cdot \hat{\boldsymbol{n}}]\!]. \tag{A13}$$

### 3. Thin-film approximation

The thin-film analysis is used to simplify the equations in the model when the longitudinal dimensions are large compared to the transverse. The destabilizing electrical stress is given by $\tau_e = \epsilon_0 \phi_0^2 / h_0^2$ and the stress due to surface tension is given by $\gamma h_0 / L^2$, where $h_0$ is the characteristic length scale in the transverse $y$ direction and $L$ is the characteristic length scale in the longitudinal $x$ direction. A balance of these two stresses gives the natural length scale for the instability which is

$$L = \left(\frac{\gamma h_0^3}{\epsilon_0 \phi_0^2}\right)^{1/2}. \tag{A14}$$

A ratio of the two length scales $\delta$ can be defined as

$$\delta = \frac{h_0}{L} = \left(\frac{\epsilon_0 \phi_0^2}{\gamma h_0}\right)^{1/2}. \tag{A15}$$

The thin-film approximation assumes that this parameter is very small. Therefore, asymptotically expanding all the equations in $\delta$ and retaining only the order one terms simplifies the analysis to a great extent. The simplified equations resulting from the thin-film approximation are listed in the following subsections.

#### *a. Governing equations*

From the above argument, the length is scaled by $h_0$ (the initial thickness of the lower fluid) and $h_0/\delta$ in the normal and tangential directions, respectively. The velocity in the $x$ direction is scaled by $\epsilon_0 \phi_0^2 \delta / (\mu_2 h_0)$, where $\epsilon_0$ is the permittivity of vacuum, $\phi_0$ is the rms value of the applied potential, and $\mu_2$ is the viscosity of the lower fluid. The scaling for the velocity in the normal direction is calculated from the continuity equation (A1) as $\epsilon_0 \phi_0^2 \delta^2 / (\mu_2 h_0)$. Substituting these scalings in the momentum balance equation for the $x$ direction gives the scaling for pressure as $\epsilon_0 \phi_0^2 / h_0^2$. $u$ and $v$ are the velocities in the $x$ and $y$ directions, respectively. The momentum balance equations (A2) with the above-mentioned scalings reduce to

$$-\partial_x p_i + C_i \partial_y^2 u_i = 0, \tag{A16}$$

while the $y$-direction momentum equation becomes

$$\partial_y p_i = 0. \tag{A17}$$

Using $\phi_0$, the rms of the applied potential, to scale the potential, the Laplace equation for potential (A3) reduces to

$$\partial_y^2 \phi_i = 0. \tag{A18}$$

#### *b. Boundary conditions*

The boundary conditions as mentioned in Appendix Sec. A 2 are scaled using the terms listed in the previous sections. At the interface, the velocities are continuous in the normal and tangential directions, i.e.,

$$v_1 = v_2, \tag{A19}$$

$$u_1 = u_2. \tag{A20}$$

The stresses are balanced in the normal and tangential directions. In the normal direction the stresses satisfy Eq. (A6). On substituting the values of the stresses [Eqs. (A8) and (A9)]

and scaling the variables, the equations reduce to

$$\left[\left[-p+\frac{1}{2}\epsilon(\partial_y\phi)^2\right]\right]=-\frac{\gamma h_0\delta^2}{\epsilon_0\phi_0^2}\partial_x^2 h. \tag{A21}$$

The coefficient term $\gamma h_0\delta^2/(\epsilon_0\phi_0^2)$ on the right-hand side is order 1 and, hence, the equation reduces to

$$\left[\left[-p+\frac{1}{2}\epsilon(\partial_y\phi)^2\right]\right]=-\partial_x^2 h. \tag{A22}$$

The balance of stresses in the tangential direction is given by

$$[\![\mu_r\partial_y u+\epsilon\partial_y\phi(\partial_y\phi\partial_x h+\partial_x\phi)]\!]=0. \tag{A23}$$

A balance of the tangential component of the field gives the continuity of the potentials across the interface

$$\phi_1=\phi_2 \tag{A24}$$

and the balance of the normal component of electric field gives

$$[\![-\epsilon_i\partial_y\phi_i]\!]=q. \tag{A25}$$

The dynamics of the position of the interface and the interfacial charge is given by the kinematic condition and the charge conservation equation, respectively,

$$\Omega\partial_t h+u_1\partial_x h=v_2, \tag{A26}$$

$$\Omega\partial_t q+\partial_x(qu)=[\![S_i\partial_y\phi_i]\!], \tag{A27}$$

where $S_1, S_2$ are the nondimensional conductivities and $\Omega$ is the nondimensional frequency equal to $\mu_2\omega h_0^2/(\epsilon_0\phi_0^2\delta^2)$ for ac fields and is equal to 1 for dc fields due to the different scaling for time in both these cases.

The boundary conditions and the governing equations are solved such that all the system variables like $u, v, \phi$ are in terms of the position of the interface $h(x,t)$. The procedure followed is as described by Shankar and Sharma [11] for dc fields and Roberts and Kumar [18] for ac fields. Initially, the governing equation (A18) is solved using the boundary conditions $\phi_1=0$ at $y=\beta$, $\phi_2=-1$ or $\sqrt{2}\cos(t)$ (for dc and ac fields, respectively) at $y=-1$, and Eqs. (A24) and (A25) to get expressions for the potentials in the two fluids ($\phi_1$ and $\phi_2$) and the interfacial charge ($q$) [Eqs. (44) and (45) from Shankar and Sharma [11]]. The $x$-direction Navier-Stokes equation [Eq. (A16)], the boundary conditions $u_1=0$ and $u_2=0$ at $y=-1$ and $y=\beta$, respectively, and Eqs. (A20) and (A23) are used to get expressions for $u_i$, the velocities in the two fluids, in the tangential direction. The pressure term is obtained from Eq. (A22). These expressions are then substituted in Eqs. (A26) and (A27) which give the evolution of the interface and the interfacial charge with time.

#### 4. Linear stability analysis

##### *a. dc fields*

The evolution equations obtained after following the procedure outlined in Sec. A 3b are reduced to linear differential equations by addition of perturbations assumed to be infinitesimal and in the normal mode form. That is, if $\tilde{m}$ is the perturbation variable

$$\tilde{m}(x,y,t)=\int \hat{m}(y,t)\,exp(ikx)dk, \tag{A28}$$

where $\hat{m}(y,t)$ is the amplitude of the perturbation and $k$ is the wave number of the perturbation. In the case of dc fields, the time dependence of perturbation amplitude is assumed to be of the form $e^{st}$, where $s$ is the growth rate of the perturbation. A dispersion relation of $s$ as a function of $k$, dependent on other system parameters like $\beta$, $\mu_r$, $\epsilon_1$, $\epsilon_2$, $S_1$, and $S_2$, is obtained. The sign of $s$ decides the stability of the system. A negative $s$ indicates a stable system, whereas the system is rendered unstable if $s$ is positive. The details of the TFA, of the dc fields induced instability, are well outlined by Shankar and Sharma [11].

##### *b. Alternating fields: Floquet theory*

We next study the instabilities in the system subjected to an ac field $\phi_p\cos(\omega t)$ (where $\phi_p=\sqrt{2}\phi_0$). The evolution equations for interfacial amplitude and interfacial charge have periodic terms and Floquet theory is employed to analyze the stability.

The set of differential equations is expressed by

$$\dot{x}=L(t)x,$$

where $L(t)$ is the matrix with periodic coefficients of period $T$. Assuming that $X(t)$ is a solution to this set of differential equations, we have $X(t+T)$ also to be a solution of the above set of differential equations. Moreover, $X(t+T)$ can be written as a linear combination of $X(t)$

$$X(t+T)=AX(t).$$

According to Floquet theory, it is the eigenvalues of the coefficient matrix $A$ that indicate if the system is stable or otherwise.

To find these set of eigenvalues, the set of ordinary differential equations are numerically integrated with the initial condition of $X(0)=I$ (where $I$ is the identity matrix) to get

$$a_{ij}=\exp\int_0^T l_{ij}(t)dt.$$

The eigenvalues of the matrix $A(a_{ij})$ give the *Floquet exponent* $\lambda_f$, from which the growth rate can be calculated as

$$s=\frac{\ln(\lambda_f)}{T}. \tag{A29}$$

For the TFA we use the evolution equations of the interface position [Eq. (A26)] and the charge conservation [Eq. (A27)] obtained after carrying out the procedure outlined in appendix Sec. A 3b and numerically integrate them from 0 to $T$ to obtain the matrix $L$ and, hence, the growth rate [using Eq. (A29)]. The present TFA thus differs slightly from the TFA conducted by Roberts and Kumar [18], where the perturbation quantities are expressed as Floquet expansions in terms of the Floquet exponent and the Floquet harmonic parameter.

## APPENDIX B: RESULTS FROM THE EXPERIMENTS

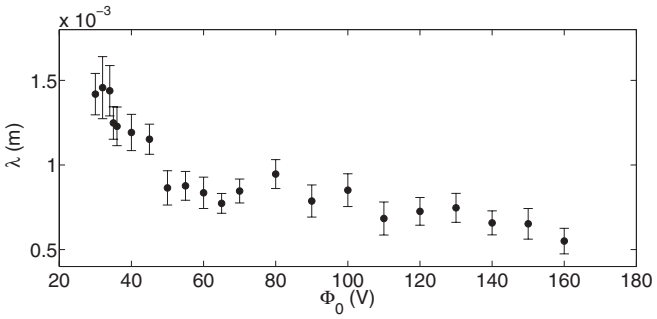


FIG. 8. Variation of the wavelength of the instability ($\lambda$) as a function of applied voltage ($\phi_0$) as obtained from experiments.

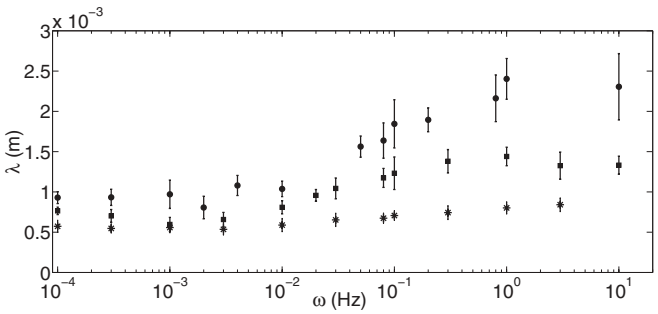


FIG. 9. Variation of the wavelength of the instability ($\lambda$) as a function of frequency ($\omega$) of the applied alternating field as obtained from experiments. •, ■, and ∗ correspond to 35, 70, and 140 V, respectively.

## APPENDIX C: ELECTRICAL CONDUCTIVITY DATA OF SILICON OIL

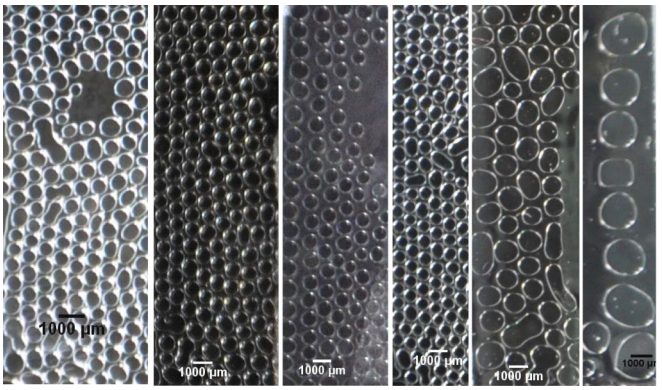


FIG. 10. Images of the instability in the form of columns rising from the pdms film and seen from the top view at different voltages. Starting from the left, the images are at 140 V and 1 mHz, 70 V and 1 mHz, 35 V and dc, 140 V and 0.3 Hz, 70 V and 10 Hz and 35 V and 1 Hz, respectively.

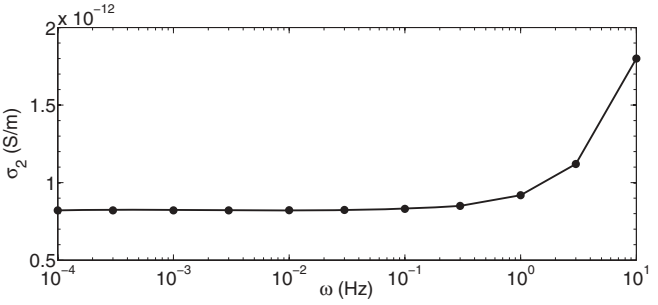


FIG. 11. The variation of conductivity ($\sigma_2$) of the polydimethylsiloxane 200 fluid of 30 000 cSt viscosity with varying frequency ($\omega$).


[1] E. Schaffer, T. Thurn-Albrecht, T. P. Russell, and U. Steiner, Nature **403**, 874 (2000).
[2] Z. Lin, T. Kerle, S. M. Baker, D. A. Hoagland, E. Schaffer, U. Steiner, and T. P. Russell, J. Chem. Phys. **114**, 2377 (2001).
[3] Z. Lin, T. Kerle, T. P. Russell, E. Schaffer, and U. Steiner, Macromolecules **35**, 3971 (2002).
[4] M. D. Morariu, Z. Lin, T. P. Russell, and U. Steiner, Nature **2**, 48 (2002).
[5] K. A. Leach, S. Gupta, M. D. Dickey, C. G. Wilson, and T. P. Russell, Chaos **15**, 047506 (2005).
[6] M. D. Dickey, S. Gupta, K. A. Leach, E. Collister, C. G. Willson, and T. P. Russel, Langmuir **22**, 4315 (2006).
[7] M. D. Dickey, A. Raines, E. Collister, R. T. Bonnecaze, S. V. Sreenivasan, and C. G. Wilson, J. Mater. Sci. **43**, 117 (2008).
[8] P. Goldberg-Oppenheimer and U. Steiner, Small **6**, 1248 (2010).
[9] L. F. Pease and W. B. Russel, J. Non-Newtonian Fluid Mech. **102**, 233 (2002).
[10] L. F. Pease and W. B. Russel, J. Chem. Phys. **118**, 3790 (2003).
[11] V. Shankar and A. Sharma, J. Colloid Interface Sci. **274**, 294 (2004).
[12] R. V. Craster and O. K. Matar, Phys. Fluids **17**, 032104 (2005).
[13] R. Verma, A. Sharma, K. Kargupta, and J. Bhaumik, Langmuir **21**, 3710 (2005).
[14] N. Wu and W. B. Russel, Appl. Phys. Lett. **86**, 241912 (2005).
[15] E. Schaffer, T. Thurn-Albrecht, T. P. Russell, and U. Steiner, Europhys. Lett. **53**, 518 (2001).
[16] N. Arun, A. Sharma, P. S. G. Pattader, I. Banerjee, H. M. Dixit, and K. S. Narayan, Phys. Rev. Lett. **102**, 254502 (2009).
[17] J. Mark, *Polymer Data Handbook* (Oxford University Press, Oxford, UK, 1999).
[18] S. A. Roberts and S. Kumar, J. Fluid Mech. **631**, 255 (2009).
[19] P. Gambhire and R. M. Thaokar, Eur. Phys. J. E **34**, 84 (2011).
[20] P. Gambhire and R. M. Thaokar, Phys. Fluids **22**, 064103 (2010).
[21] D. A. Saville, Annu. Rev. Fluid Mech. **29**, 27 (1997).